PROCEEDINGS OF SPIE

SPIEDigitalLibrary.org/conference-proceedings-of-spie

Compact setup for SIMO measurements of slab interconnects and correlation with PEDOT:PSS nanostructure morphology

Watanabe, Reid, Nelson, David, Nirenberg, Shaya, Vuong, Luat

Reid Watanabe, David Nelson, Shaya Nirenberg, Luat T. Vuong, "Compact setup for SIMO measurements of slab interconnects and correlation with PEDOT:PSS nanostructure morphology," Proc. SPIE 11389, Micro- and Nanotechnology Sensors, Systems, and Applications XII, 113892X (20 May 2020); doi: 10.1117/12.2559034



Event: SPIE Defense + Commercial Sensing, 2020, Online Only

Compact Setup for SIMO Measurements of Slab Interconnects and Correlation with PEDOT:PSS Nanostructure Morphology

Reid Watanabe, David Nelson, Shaya Nirenberg, and Luat T. Vuong*
Department of Mechanical Engineering,
University of California at Riverside, Riverside, CA 92521

0. Abstract

We demonstrate a compact, portable and reliable, poor-man's 8-channel interconnect and measure, in the 50-100MHz VHF radiofrequency range, the path-dependent voltage transfer function across drop-cast poly(3,4-ethylenedioxythiophene) polystyrene sulfonate (PEDOT:PSS). The setup may be inexpensively deployed for single-input-multiple-output (SIMO) self-sensing materials with computational impedance tomography algorithms. We test our setup with PEDOT:PSS samples that are dried in a static magnetic field. These samples exhibit anisotropic electrical conductivities and nanostructure morphologies. Voltages across the sample vary 2dB as a result of this anisotropy. This processing-dependent anisotropy of PEDOT:PSS may be useful in future efforts aimed at deconvolving the path-dependent electrical tomography measurements, as necessary for such a sensing system.

1. Introduction

Here we demonstrate a portable interconnect sensor similar to that previous demonstrated with nanocomposite materials^{1,2,3}. The concept is motivated by electrical impedance tomography schemes, where electrodes on the perimeter of a surface material are able to sense changes in the electrode interior⁴. Such schemes that originated decades ago, largely aimed at biomedical applications, are now employed in soft robotics—to register hand-gestures, in one example⁵—and self-sensing materials—for identifying damage in civil engineering structures, in another⁶. The sample electronics and Arduino controller all fit in a small box with dimensions 5cm x 7cm x 25cm.

As the sensing material, we focus on poly(3,4-ethylenedioxythiophene) polystyrene sulfonate (PEDOT:PSS), a conducting polymer that is widely used to fabricate electrodes in-situ and from solution. Larger PEDOT:PSS electrodes have lower impedance, which influences the sensing dynamic range and also dictates antenna-like functionality. Prior-reported impedance characterization shows resonant behavior at 100Hz-kHz for sub-millimeter and millimeter-sized electrodes^{7,8}, and MHz to GHz for mm-to-cm sized antennas^{9,10,11}. We focus on opaque, drop-cast mm-sized PEDOT:PSS slabs in the 50-100MHz range and demonstrate repeatable and reliable measurements. Furthermore, we measure anisotropy in the PEDOT:PSS slabs that are a result of magnetophoretic alignment.

PEDOT:PSS is one of the most commonly-deployed conducting polymers in electronics research and industry. It widely serves as an electrode material and is used in biomedical, photovoltaic, organic electronic, sensor, RFID applications, and there are additional advantages beyond being solution-processed. There is interest in PEDOT:PSS as a spintronic material 12. Since its plasma frequency is chemically tunable over several orders of magnitude across the radiofrequency spectrum, PEDOT:PSS may be a transparent conducting material in the visible range 13,14. Related to its nanometer-confined conducting and insulating channels of mixed electron-ion networks 15, PEDOT:PSS exhibits neuromorphic synaptic responses 16 associated with self-assembled nano-circuits potentially capable of massive parallel computation 17. It has recently been suggested that in this networked domain there are also electrical double layers that influence charge transport 18, which may explain unusual temporal charge transport dynamics. At a macroscopic level, the physical properties of PEDOT:PSS (electrical conductivity, refractive index) depend strongly on environmental conditions, so it is suggested that PEDOT:PSS may reliably sense changes in temperature, humidity, and gases 19,20,21,22.

We have recently studied how PEDOT:PSS conductivity is strongly anisotropic when it settles in mT-magnetic fields²³. As a result of the presence of mT-magnetic fields while the polymer sample dries, the electrical conductivity and Seebeck coefficients increase by a factor of 2 and 5, respectively. Corresponding images of the nanostructure arising from the applied magnetic fields show that, while PEDOT:PSS dries layer-by-layer inhomogeneously²⁴, the magnetophoretic changes in morphology occur through the bulk. The magnetic field-induced alignment may be similar to what others have reported in other polymers^{25,26,27}. Nevertheless, this processing-dependent anisotropy may be useful in future efforts aimed at deconvolving the path-dependent electrical properties of PEDOT:PSS in computer tomography algorithms.

2. Experimental setup

Samples are prepared on a printed circuit board (PCB) with an 8-pin configuration [Fig. 1(a)]. The PCB area is cleaned with methanol before 0.05mL PEDOT:PSS (Sigma Aldrich, 99% electronic grade) is dropped onto the presoldered PCB board. Each sample is prepared directly on the PCB where PEDOT:PSS makes electrical contact with

Micro- and Nanotechnology Sensors, Systems, and Applications XII, edited by Thomas George, M. Saif Islam, Proc. of SPIE Vol. 11389, 113892X · © 2020 SPIE · CCC code: 0277-786X/20/\$21 · doi: 10.1117/12.2559034

2 pins along each edge of a square. These pins control the orientation of the electrical measurement of the PEDOT:PSS sample. The samples are dried over a hotplate at 150C on top and next-to a neodymium magnet, where the magnetic field is 50-150mT. Ideally, pins are soldered prior to drop-casting to prevent thermal damage of PEDOT:PSS. We test two configurations: one where the PCB is on top of the magnet and the fields are perpendicular to the substrate and another where the PCB is at the magnet side and the magnetic fields are largely in-plane with the substrate. Unlike in previous experiments where we employ a Helmholz coil²³, here the magnetic fields are stronger, less uniform, and directed in different directions across the sample. The PEDOT:PSS settles at 150C for 1 hour. A reference sample is made with silver solder across the pins.

The PEDOT:PSS PCB sample fits on a small breadboard where all 8 channels are attached to three multiplexers (16-Channel Analog/Digital Multiplexer/Demultiplexer Digital MUX Breakout - CD74HC4067). This chip is like a rotary switch; it internally routes the common pin (COM in the schematic, SIG on the board) to one of 16 channel pins (CHANxx). Each MUX board is configured for 16 channels with only 5 pins [see datasheet²⁸]. We use 8 of the 16 channels so we only use 3 of the address pins (S0-S2). The MUX is capable of operating with both digital and analog signals (the voltage cannot be higher than VCC). The connections are bi-directional and allow current in either direction. To control each MUX, digital outputs are connected to the chip's address select pins and sent to the binary address of the channel.

A USB-powered Arduino (Uno R3) controls the location of the input and measured voltages on the PEDOT:PSS sample. We use 12 of the 14 Arduino's 5V I/Os to control the address pins of the three MUX boards [Figure 1b]. Each MUX connects 1 of the 8 channels to the ground, input signal, or output signal of a Liquid Instruments Moku:Lab instrument²⁹. The Moku:Lab provides testing and troubleshooting tools (oscilloscope, frequency-response analyzer, and lockin-amplifier) in a compact, mobile device. The sample and all its electrical components are housed in an aluminum box that is 5cm x 7cm x 25cm. The Moku:Lab ground is connected to the ground rail of the breadboard and the aluminum box. A plastic platform is 3D-printed for the Arduino, so the sample, breadboard, MUXes, and Arduino are organized in the box. The aluminum box encloses the compact setup, reduces electrical noise, and may be helpful for achieving thermal or humidity control of PEDOT:PSS.

An external computer sends pymoku³⁰ and pyfirmata³¹ commands to control the Moku:Lab and Arduino, respectively. The Arduino outputs voltages that determine the (ground-input-output) pin combination on the sample, which are used in the Moku:Lab time-domain and frequency-domain measurements.

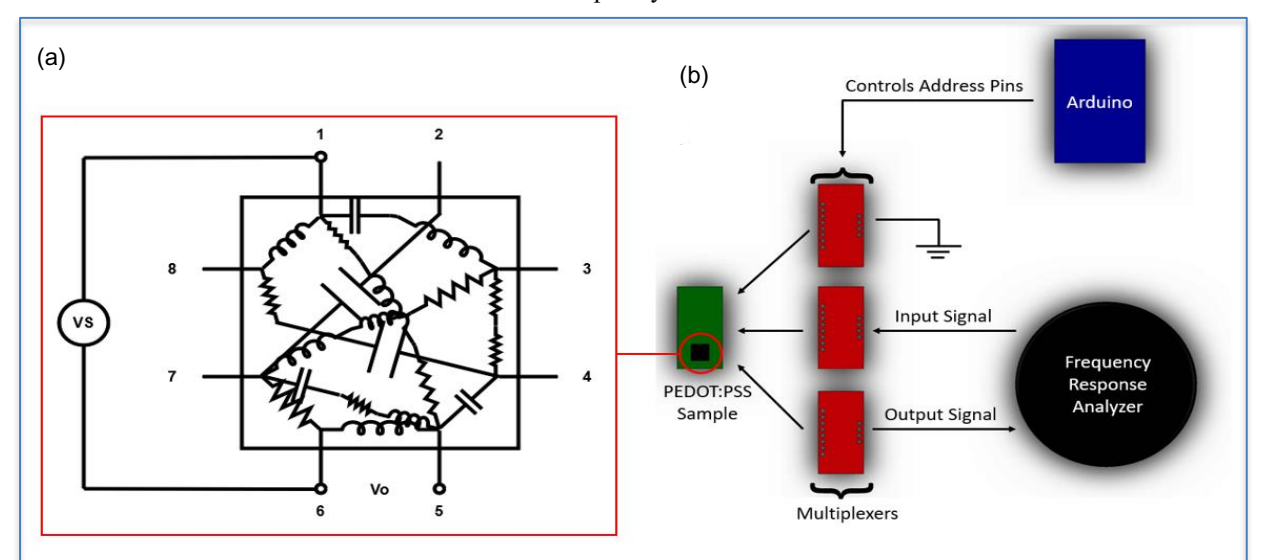


Figure 1: (a) Illustration of pin orientation on PEDOT:PSS sample. **(b)** Experimental schematic of the Arduino, multiplexers, frequency-response analyzer, and sample.

3. Measurements

i. Time-domain VHF RF Characterization

In the Moku:Lab oscilloscope mode, we illustrate considerations for high-frequency measurements. An input sinusoidal signal of 75 MHz is applied with varying peak-to-peak voltages Vpp (Ground-Input-Output Pin

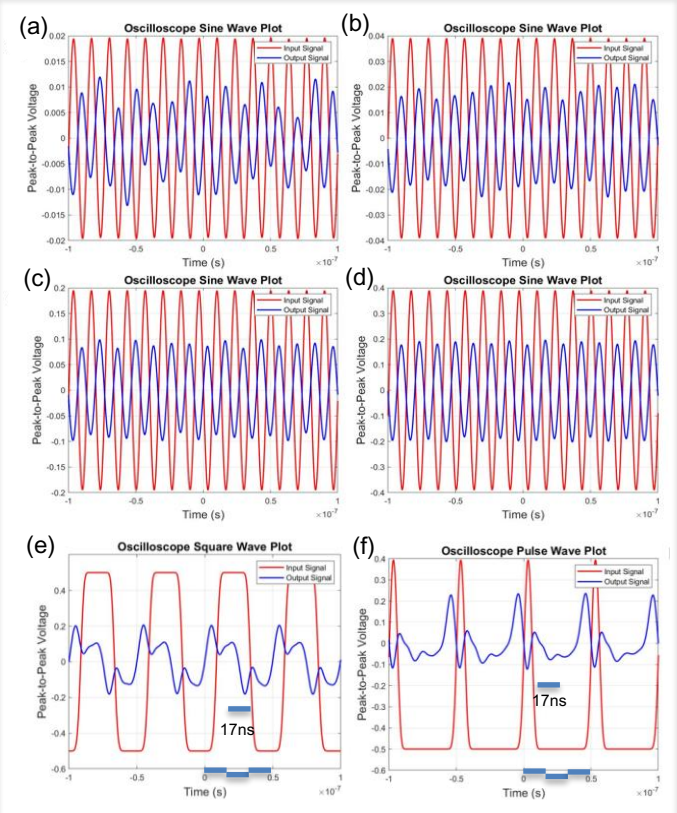


Figure 2: Sinusoidal input and output 75 MHz signals with **(a)** 50 mVpp **(b)** 100 mVpp **(c)** 500 mVpp **(d)** 1 Vpp. Phase delay is chosen so that output RMS is clear. **(e)** Square and **(f)** pulse wave input and outputs with 1 Vpp using the metal reference sample. Strong resonances at 120MHz are visible. Here, the ground-input-output combination is (1-4-2).

configuration: 1-4-2) [Fig. 2(a-d)]. As Vpp increases from 50mV to 1V, the RMS Vpp decreases from 50% to 10% of the signal Vpp and is approximately 10mVpp. The RMS implies that the sample is not fully isolated from the external circuitry, however the magnitude and phase of the output signal is reliable, as is the variation in the signal amplitude.

We note a strong resonance at 60MHz, which we expect to be related to the MUX configuration. When we replace the sample with a metal solder reference for comparison and input a repeating pulse and square wave (1Vpp), the resonant features are visible in the time-domain. The step and pulse responses show a superposition of many frequency responses, some of which are malformed. Both measurements show a strong 60MHz ringing [Fig. 2(e-f)], which is an unfavorable frequency response of the circuit. This resonance may indicate how the transfer function is distorted around 60MHz so that it may be challenging to measure absolute impedance over the sensor. However, within the scope of our tomography-related interests and relative frequency-domain measurements 50MHz-100MHz, these resonances do not influence repeatability.

ii. Frequency-Analyzer Measurements

In the Moku:Lab Bode analyzer mode, we study the frequency-domain transfer function. PEDOT:PSS sample data is referenced to metal reference data for each channel. We measure all combinations of output voltages for a specified ground for each input within one set of data. The transfer function is measured relative to one reference pin combination (1-4-2) to distill the

anisotropy across the sample.

Since PEDOT:PSS is a strongly capacitive material, we find that it is essential to ground all channels between measurements. We set the ground to one pin, and set the input and output to the same pin prior to each measurement. We subsequently set the state of the ground and input pins for the measurement, and then set the output pin. For each set of measurements, the input and ground are fixed, while the output pin is moved to the other pins with exception of the ground and input pins. After the measurement is taken for a specific pin combination, all pins are again grounded. There is a time delay of 50s after setting any new pin combination. We also pause 40s between frequency-sweep measurements and during the grounding prior to the first measurement of each set. These pauses between measurements eliminate concerns of accumulated thermal effects, since we found that without such pauses, the measurements drift.

Bode plots show the magnitude of the transfer function with different pin combinations and demonstrate anisotropy as a result of PEDOT:PSS drying in a magnetic field [Fig. 3]. These specific measurements are taken for a combination of outputs X where the ground-input-output pin layout is (1-4-X). Three sets of measurements taken 30-min apart are averaged and the standard deviations are shown with error bars. (1-4-2) is a reference. The reliability and consistency of these measurements are representative with what would be observed using other samples and measured with these particular samples on different days.

When PEDOT:PSS is dried in a magnetic field in the plane of the sample, the anisotropic diffusion of charge leads to variations of 2dB in the transfer function, which is measured at other pins across the sample. Instead, if the PEDOT:PSS is dried with a magnetic field perpendicular to the sample, there is only a 0.3dB difference in the transfer function across the sample. These measurements reflect the anisotropy (uniformity) of the samples when dried with in-plane (perpendicular) magnetic fields, and these measurements are consistent with our prior experiments²³. The

conductivity is generally higher in a direction perpendicular to the magnetic field. We remark that the measurements are repeatable to such an extent that the "bar" in the error bar is not always visible, i.e., within the thickness of the error-bar line. Small features (peaks and dips) in the Bode plot in this range are highly repeatable and are not expected to be artifacts but instead related to the nanostructure localization and temporal charge dynamics of PEDOT:PSS.

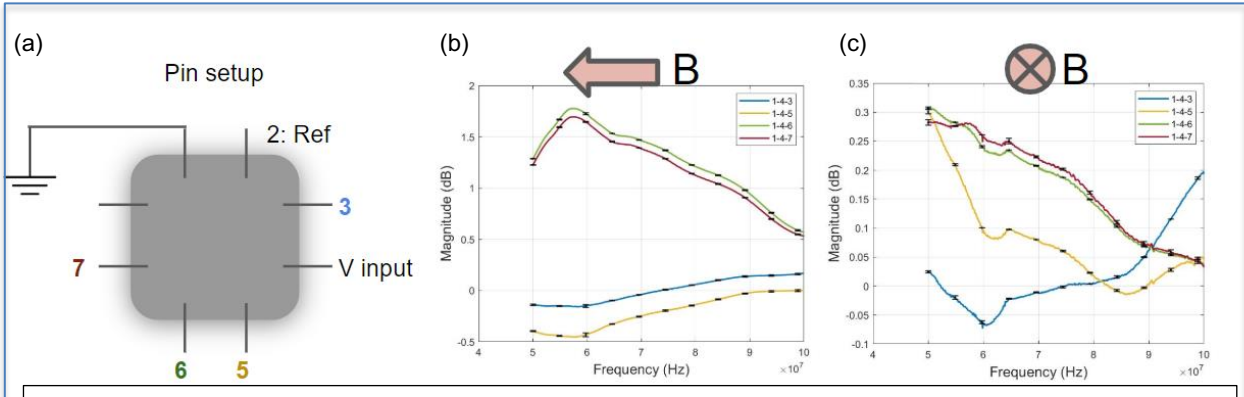


Figure 3: (a) Pin setup depicting measurement and pin orientation. Bode magnitude plot for a sinusoidal sweep 50 MHz – 100 MHz (500 mVpp) with PEDOT:PSS samples dried in a 100-mT magnetic field (b) parallel and (c) perpendicular to the PEDOT:PSS slab.

iii. Discussion of Repeatability of Measurements with PEDOT:PSS

We are interested in the very-high-frequency (VHF) range 50-100MHz of the Moku:Lab, since high-speed readout is desirable. We measure resonances of the PEDOT:PSS sample around 55-90MHz, which would accompany higher-gain sensing in this range. In spite of some perceived challenges, we achieve results that are consistent enough to characterize the anisotropy within the PEDOT:PSS. Practical challenges are related to the sensor being at a testing stage currently. When the sample and reference samples are switched in an out, we may introduce microcracks in the solder joints. Particularly at these higher frequencies, the signal fidelity is sensitive to solder micro cracks. Adjustments to the circuit often accompany a gradual onset of a weak solder-joint breakage³² or PEDOT:PSS delamination. These changes in sensor fidelity would be observed over the course of hours or days and interfere with our ability to characterize the reliability of the signal measurement, itself.

The current set up is also sensitive to changes in temperature and humidity. Over the course of hours the measurements are reliable. Measurements over the course of days show similar shapes and trends but may also exact a shift in magnitude. Ambient temperatures as well as the temperature of the sample from the resistive heating of prior measurements can influence later measurements. The Moku:Lab instrument typically requires 10 minutes to warm up. Future efforts aimed at reliable sensing may require that the temperature and humidity are controlled, however even when the temperature is not controlled, we are confident that the relative transfer function in the anisotropic sample transfer function are well preserved.

If the solder joints are securely soldered and the temperature and humidity are stable, then frequency-domain impedance measurements from 50-100MHz are very stable and show interesting and repeatable features.

4. Conclusion

We successful build a compact, portable, SIMO sensor in the VHF 50-100MHz range and characterize some of the issues for working in this range with a sensor material such as PEDOT:PSS. Our results indicate potential for PEDOT:PSS as a reliable sensing material. With some care, we have shown that it is possible to achieve highly repeatable measurements to such an extent that we may begin to relate nanostructure morphology with charge carrier temporal dynamics. Time-domain measurements show resonant features from external circuits (i.e., MUXes) and 0.01Vpp noise. These features do not affect the repeatability of relative frequency-domain measurements with the Moku:Lab. In order to achieve this level of repeatability, we are careful to ground the sample and eliminate any charge that may accumulate from the MUX switching. We also pause between measurements to ensure that the sample returns to equilibrium (ambient temperature) between measurements.

We confirm the strong anisotropic charge diffusion that results from PEDOT:PSS when drop-cast samples are dried and annealed in a magnetic field. In the 50-100MHz range, the magnitude of the transfer function across the PEDOT:PSS varies from 0.3dB to 2dB, depending on the magnetophoretically-induced anisotropy. We believe that this morphological control over the sensing material is valuable for signal processing as well as useful in computer

tomography calculations³³. This SIMO setup may be employed beyond sensing to correlate morphology and charge temporal dynamics^{34,35}, to develop more advanced models of nanocomposite impedance³⁶, and to develop neuromorphic reservoir computing applications³⁷.

5. Acknowledgements

The authors gratefully acknowledge funding from NSF DMR 1921034.

6. References

¹ J.-W. Han, B. Kim, Y. C. Park, and M. Meyyappan, "Note: Two-dimensional resistivity mapping method for characterization of thin films and nanomaterials," Review of Scientific Instruments, vol. 82, no. 8, p. 86117, Aug. 2011 [Online]. Available: http://dx.doi.org/10.1063/1.3626797

² T.-C. Hou, K. J. Loh, and J. P. Lynch, "Electrical impedance tomography of carbon nanotube composite materials," in Sensors and Smart Structures Technologies for Civil, Mechanical, and Aerospace Systems 2007, 2007, doi: 10.1117/12.715663 [Online]. Available: http://dx.doi.org/10.1117/12.715663

³ D.-I. Moon et al., "A Single Input Multiple Output (SIMO) Variation-Tolerant Nanosensor," ACS Sensors, vol. 3, no. 9, pp. 1782–1788, Aug. 2018, doi: 10.1021/acssensors.8b00510. [Online]. Available: http://dx.doi.org/10.1021/acssensors.8b00510

⁴ B. Brown, "Electrical impedance tomography (EIT): a review," Journal of Medical Engineering & Technology, vol. 27, no. 3, pp. 97–108, Jan. 2003, doi: 10.1080/0309190021000059687. [Online]. Available: http://dx.doi.org/10.1080/0309190021000059687

⁵ Y. Zhang, R. Xiao, and C. Harrison, "Advancing Hand Gesture Recognition with High Resolution Electrical Impedance Tomography," in Proceedings of the 29th Annual Symposium on User Interface Software and Technology, 2016, doi: 10.1145/2984511.2984574 [Online]. Available: http://dx.doi.org/10.1145/2984511.2984574
⁶ H. Hassan and T. N. Tallman, "Damage sizing in self-sensing materials using a genetic algorithm-supplemented electrical impedance tomography formulation," in Sensors and Smart Structures Technologies for Civil, Mechanical, and Aerospace Systems 2020, 2020 [Online]. Available: http://dx.doi.org/10.1117/12.2557025

⁷ D. A. Koutsouras et al., "Probing the Impedance of a Biological Tissue with PEDOT:PSS-Coated Metal Electrodes: Effect of Electrode Size on Sensing Efficiency," Advanced Healthcare Materials, vol. 8, no. 23, p. 1901215, Nov. 2019 [Online]. Available: http://dx.doi.org/10.1002/adhm.201901215

⁸ C. Chen, A. Kine, R. D. Nelson, and J. C. LaRue, "Impedance spectroscopy study of conducting polymer blends of PEDOT:PSS and PVA," Synthetic Metals, vol. 206, pp. 106–114, Aug. 2015, doi: 10.1016/j.synthmet.2015.05.003. [Online]. Available: http://dx.doi.org/10.1016/j.synthmet.2015.05.003

⁹ H. Zhou, S. Li, S. Chen, Q. Zhang, W. Liu, and X. Guo, "Enabling Low Cost Flexible Smart Packaging System With Internet-of-Things Connectivity via Flexible Hybrid Integration of Silicon RFID Chip and Printed Polymer Sensors," IEEE Sensors Journal, vol. 20, no. 9, pp. 5004–5011, May 2020 [Online]. Available: http://dx.doi.org/10.1109/JSEN.2020.2966011

¹⁰ K. Guerchouche, E. Herth, L. E. Calvet, N. Roland, and C. Loyez, "Conductive polymer based antenna for wireless green sensors applications," Microelectronic Engineering, vol. 182, pp. 46–52, Oct. 2017 [Online]. Available: http://dx.doi.org/10.1016/j.mee.2017.08.007

¹¹ Z. Li et al., "All-organic flexible fabric antenna for wearable electronics," Journal of Materials Chemistry C, vol. 8, no. 17, pp. 5662–5667, 2020, doi: 10.1039/d0tc00691b. [Online]. Available: http://dx.doi.org/10.1039/d0tc00691b

¹² M. M. Qaid, M. R. Mahani, J. Sinova, and G. Schmidt, "Quantifying the inverse spin-Hall effect in highly doped PEDOT:PSS," Physical Review Research, vol. 2, no. 1, Feb. 2020, doi: 10.1103/physrevresearch.2.013207. [Online]. Available: http://dx.doi.org/10.1103/PhysRevResearch.2.013207

¹³ M. Zhang, S. Höfle, J. Czolk, A. Mertens, and A. Colsmann, "All-solution processed transparent organic light emitting diodes," Nanoscale, vol. 7, no. 47, pp. 20009–20014, 2015, doi: 10.1039/c5nr05820a. [Online]. Available: http://dx.doi.org/10.1039/C5NR05820A

¹⁴ T. Kim et al., "Megahertz-wave-transmitting conducting polymer electrode for device-to-device integration," Nature Communications, vol. 10, no. 1, Feb. 2019 [Online]. Available: http://dx.doi.org/10.1038/s41467-019-08552-z

¹⁵ A. V. Volkov et al., "Understanding the Capacitance of PEDOT:PSS," Advanced Functional Materials, vol. 27, no. 28, p. 1700329, May 2017 [Online]. Available: http://dx.doi.org/10.1002/adfm.201700329

- ¹⁶ P. Gkoupidenis, N. Schaefer, B. Garlan, and G. G. Malliaras, "Neuromorphic Functions in PEDOT:PSS Organic Electrochemical Transistors," Advanced Materials, vol. 27, no. 44, pp. 7176–7180, Oct. 2015, doi: 10.1002/adma.201503674. [Online]. Available: http://dx.doi.org/10.1002/adma.201503674
- ¹⁷ S. Pecqueur, D. Vuillaume, and F. Alibart, "Perspective: Organic electronic materials and devices for neuromorphic engineering," Journal of Applied Physics, vol. 124, no. 15, p. 151902, Oct. 2018, doi: 10.1063/1.5042419. [Online]. Available: http://dx.doi.org/10.1063/1.5042419
- ¹⁸ A. V. Volkov et al., "Understanding the Capacitance of PEDOT:PSS," Advanced Functional Materials, vol. 27, no. 28, p. 1700329, May 2017, doi: 10.1002/adfm.201700329. [Online]. Available: http://dx.doi.org/10.1002/adfm.201700329
- ¹⁹ E. S. Muckley et al., "New Insights on Electro-Optical Response of Poly(3,4-ethylenedioxythiophene):Poly(styrenesulfonate) Film to Humidity," ACS Applied Materials & Interfaces, vol. 9, no. 18, pp. 15880–15886, Apr. 2017, doi: 10.1021/acsami.7b03128. [Online]. Available: http://dx.doi.org/10.1021/acsami.7b03128
- ²⁰ S. Manzari, C. Occhiuzzi, S. Nawale, A. Catini, C. Di Natale, and G. Marrocco, "Polymer-doped UHF RFID tag for wireless-sensing of humidity," in 2012 IEEE International Conference on RFID (RFID), 2012, doi: 10.1109/rfid.2012.6193039 [Online]. Available: http://dx.doi.org/10.1109/RFID.2012.6193039
- ²¹ I. W. Kwon, H. J. Son, W. Y. Kim, Y. S. Lee, and H. C. Lee, "Thermistor behavior of PEDOT:PSS thin film," Synthetic Metals, vol. 159, no. 12, pp. 1174–1177, Jun. 2009, doi: 10.1016/j.synthmet.2009.02.006. [Online]. Available: http://dx.doi.org/10.1016/j.synthmet.2009.02.006
- ²² B. Kim, T. J. Norman, R. S. Jones, D. Moon, J. Han, and M. Meyyappan, "Carboxylated Single-Walled Carbon Nanotube Sensors with Varying pH for the Detection of Ammonia and Carbon Dioxide Using an Artificial Neural Network," ACS Applied Nano Materials, vol. 2, no. 10, pp. 6445–6451, Sep. 2019, doi: 10.1021/acsanm.9b01401. [Online]. Available: http://dx.doi.org/10.1021/acsanm.9b01401
- ²³ V. A. Zarubin et al., "Improved Anisotropic Thermoelectric Behavior of Poly(3,4-ethylenedioxythiophene):Poly(styrenesulfonate) via Magnetophoresis," ACS Omega, vol. 3, no. 10, pp. 12554–12561, Oct. 2018 [Online]. Available: http://dx.doi.org/10.1021/acsomega.8b00999
- ²⁴ M. Kemerink, S. Timpanaro, M. M. de Kok, E. A. Meulenkamp, and F. J. Touwslager, "Three-Dimensional Inhomogeneities in PEDOT:PSS Films," The Journal of Physical Chemistry B, vol. 108, no. 49, pp. 18820–18825, Dec. 2004, doi: 10.1021/jp0464674. [Online]. Available: http://dx.doi.org/10.1021/jp0464674
- ²⁵ Y. Rokhlenko et al., "Magnetic Alignment of Block Copolymer Microdomains by Intrinsic Chain Anisotropy," Physical Review Letters, vol. 115, no. 25, Dec. 2015, doi: 10.1103/physrevlett.115.258302. [Online]. Available: http://dx.doi.org/10.1103/PhysRevLett.115.258302
- ²⁶ M. Gopinadhan et al., "Controlling orientational order in block copolymers using low-intensity magnetic fields," Proceedings of the National Academy of Sciences, vol. 114, no. 45, pp. E9437–E9444, Oct. 2017, doi: 10.1073/pnas.1712631114. [Online]. Available: http://dx.doi.org/10.1073/pnas.1712631114
- ²⁷ X. Li, D. Hou, and G. Chen, "Magnetic field effect on polaron recombination in conjugated polymers," Physica E: Low-dimensional Systems and Nanostructures, vol. 108, pp. 1–6, Apr. 2019, doi: 10.1016/j.physe.2018.10.015. [Online]. Available: http://dx.doi.org/10.1016/j.physe.2018.10.015
- ²⁸ https://www.ti.com/lit/ds/symlink/cd74hc4067.pdf
- ²⁹ https://liquidinstruments.com/moku-lab/
- 30 https://github.com/liquidinstruments/pymoku
- 31 https://pypi.org/project/pyFirmata/
- ³² D. Kwon, M. H. Azarian, and M. G. Pecht, "Detection of solder joint degradation using RF impedance analysis," in 2008 58th Electronic Components and Technology Conference, 2008, doi: 10.1109/ectc.2008.4550035 [Online]. Available: http://dx.doi.org/10.1109/ECTC.2008.4550035
- ³³ S. J. Hamilton, M. Lassas, and S. Siltanen, "A direct reconstruction method for anisotropic electrical impedance tomography," Inverse Problems, vol. 30, no. 7, p. 75007, Jun. 2014, doi: 10.1088/0266-5611/30/7/075007. [Online]. Available: http://dx.doi.org/10.1088/0266-5611/30/7/075007
- ³⁴ S. Buonocore and F. Semperlotti, "Tomographic imaging of non-local media based on space-fractional diffusion models," Journal of Applied Physics, vol. 123, no. 21, p. 214902, Jun. 2018, doi: 10.1063/1.5026789. [Online]. Available: http://dx.doi.org/10.1063/1.5026789
- ³⁵ S. J. Hamilton, M. Lassas, and S. Siltanen, "A direct reconstruction method for anisotropic electrical impedance tomography," Inverse Problems, vol. 30, no. 7, p. 75007, Jun. 2014, doi: 10.1088/0266-5611/30/7/075007. [Online]. Available: http://dx.doi.org/10.1088/0266-5611/30/7/075007

³⁶ S. Pecqueur, I. Lončarić, V. Zlatić, D. Vuillaume, and Ž. Crljen, "The non-ideal organic electrochemical transistors impedance," Organic Electronics, vol. 71, pp. 14–23, Aug. 2019, doi: 10.1016/j.orgel.2019.05.001. [Online]. Available: http://dx.doi.org/10.1016/j.orgel.2019.05.001

³⁷ G. Tanaka et al., "Recent advances in physical reservoir computing: A review," Neural Networks, vol. 115, pp. 100–123, Jul. 2019 [Online]. Available: http://dx.doi.org/10.1016/j.neunet.2019.03.005